A possible role of the junctional face protein JP-45 in modulating Ca^{2+} release in skeletal muscle

E. Gouadon[1], R. P. Schuhmeier[1], D. Ursu[1], A. A. Anderson[2], S. Treves[2], F. Zorzato[3], F. Lehmann-Horn[1] and W. Melzer[1]

[1] *University of Ulm, Department of Applied Physiology, Albert-Einstein-Allee 11, D-89069 Ulm, Germany*
[2] *Basel University Hospital, Departments of Anaesthesia and Research, Hebelstrasse 20, 4031 Basel, Switzerland*
[3] *University of Ferrara, Department of Experimental and Diagnostic Medicine, Via Borsari 46, 44100 Ferrara, Italy*

We investigated the functional role of JP-45, a recently discovered protein of the junctional face membrane (JFM) of skeletal muscle. For this purpose, we expressed JP-45 C-terminally tagged with the fluorescent protein DsRed2 by nuclear microinjection in myotubes derived from the C2C12 skeletal muscle cell line and performed whole-cell voltage-clamp experiments. We recorded in parallel cell membrane currents and Ca^{2+} signals using fura-2 during step depolarization. It was found that properties of the voltage-activated Ca^{2+} current were not significantly changed in JP-45–DsRed2-expressing C2C12 myotubes whereas the amplitude of depolarization-induced Ca^{2+} transient was decreased compared to control myotubes expressing only DsRed2. Converting Ca^{2+} transients to Ca^{2+} input flux using a model fit approach to quantify Ca^{2+} removal, the change could be attributed to an alteration in voltage-activated Ca^{2+} permeability rather than to altered removal properties or a lower Ca^{2+} content of the sarcoplasmic reticulum (SR). Determining non-linear capacitive currents revealed a reduction of Ca^{2+} permeability per voltage-sensor charge. The results may be explained by a modulatory effect of JP-45 related to its reported *in vitro* interaction with the dihydropyridine receptor and the SR Ca^{2+} binding protein calsequestrin (CSQ).

(Resubmitted 23 December 2005; accepted 18 January 2006; first published online 19 January 2006)
Corresponding author W. Melzer: University of Ulm, Department of Applied Physiology, Albert-Einstein-Allee 11, D-89069 Ulm, Germany. Email: werner.melzer@uni-ulm.de

A rapid rise in intracellular Ca^{2+} concentration activates force in skeletal muscle cells (Melzer *et al.* 1995; Bers, 2001). Ca^{2+} is stored in the terminal cisternae of the sarcoplasmic reticulum (SR) and buffered by the low-affinity, high-capacity Ca^{2+} binding protein calsequestrin (CSQ). It is released under the control of the membrane potential of the transverse tubules (TTs), which conduct the action potential from the cell surface into the cell. The released Ca^{2+} is bound by its target protein troponin C on the actin filament to induce force and is re-sequestered to the SR by the SR transport Ca^{2+} ATPase.

The Ca^{2+} mobilization involves opening of ryanodine receptors (RyRs) in the membrane region of the terminal cisternae facing the TTs, termed 'junctional face membrane' (JFM). Voltage-dependent activation of dihydropyridine receptors (DHPRs) in the TT membrane leads to activation of the RyRs by conformational coupling across the junctional gap separating the JFM and TT. The α_1-subunit of the DHPR serves as the voltage sensor in the Ca^{2+} release process. It is currently thought that step depolarization in voltage-clamp experiments first rapidly activates a flux of Ca^{2+} from the SR and then very slowly a Ca^{2+} inward flux from the TTs (L-type Ca^{2+} current) (Brum *et al.* 1987; Friedrich *et al.* 1999; Szentesi *et al.* 2001). Both depend on the voltage-sensing properties of the DHPRs (Melzer *et al.* 1995).

In addition to the main constituents of the Ca^{2+} signalling process, a number of proteins with still ill-defined functions have been identified, which are associated with the α_1-subunit of the DHPR in the TT membrane (Walker & De Waard, 1998; Arikkath & Campbell, 2003) or with the RyRs in the JFM (Caswell *et al.* 1991; Knudson *et al.* 1993; Guo & Campbell, 1995; Jones *et al.* 1995; MacKrill, 1999). One of these proteins is a recently discovered constituent of the JFM with an apparent molecular mass of 45 kDa that has been termed JP-45 (Zorzato *et al.* 2000). Co-localization of JP-45 and RyR1 has been indicated by an overlapping striation pattern in adult rat muscle fibres (Anderson *et al.* 2003). The protein contains 332 amino-acid residues and exhibits a single *trans*-membrane segment. The protein is highly charged, in particular the domain facing the SR lumen. The larger number of positively charged amino-acid residues makes it a basic protein. Co-immunoprecipitation

 DOI: 10.1113/jphysiol.2005.104406

experiments demonstrated *in vitro* interaction with the DHPR and CSQ (Anderson *et al.* 2003). This raises the question of whether JP-45 acts as a modulator of voltage-controlled Ca^{2+} entry or Ca^{2+} release. So far, no functional data are available and it is not known whether JP-45 exhibits interactions with components of the Ca^{2+} release system *in vivo*. One approach to assess possible functional effects on muscle excitation–contraction (EC) coupling is the over-expression of the protein in normal muscle cells.

For the present experiments, we chose the skeletal muscle cell line C2C12. C2C12 myotubes show great similarities in Ca^{2+} signalling to adult muscle fibres (Schuhmeier & Melzer, 2004; Ursu *et al.* 2005) and can therefore serve as a model system for mature EC coupling. We injected plasmids encoding fluorescent fusion proteins of JP-45 into the nuclei of C2C12 myotubes, observed the intracellular expression pattern and studied function (i.e. Ca^{2+} inward current, gating charge movements and Ca^{2+} release) under voltage-clamp conditions. The results suggest that JP-45 alters the voltage-controlled Ca^{2+} permeability of the SR.

Methods

Cell culture

C2C12 cells, purchased from the American Tissue Culture Collection (ATCC, Manassas, VA, USA), were cultured in growth medium (Dulbecco's modified Eagle's medium, DMEM), supplemented with 10% fetal bovine serum as described by Schuhmeier *et al.* (2003). To induce myotube formation and differentiation, cells were cultured in collagen-coated flasks containing DMEM supplemented with 2% horse serum. One day prior to experiments, myotubes were transferred from flasks onto collagen- and carbon-coated coverslips using a mild trypsin treatment.

Expression plasmids

The following plasmids were purchased from Clontech BD Biosciences (Heidelberg, Germany): pEGFP-C1, pDsRed2-N3 and pDsRed2-ER. pDsRed2-ER has been designed for fluorescent labelling of the endoplasmic reticulum (ER). A plasmid (pGFP-α_{1C}) encoding the green fluorescent protein (GFP)-tagged α_1-subunit of the cardiac L-type Ca^{2+} channel ($Ca_V1.2$) (Grabner *et al.* 1998) was kindly provided by M. Grabner and B. E. Flucher (Innsbruck Medical University).

The coding sequence of JP-45 (Anderson *et al.* 2003) was inserted 'in frame' into the red fluorescent protein coding vector pDsRed2-N3 and into the enhanced green fluorescent protein coding vector pEGFP-C1 resulting in plasmids encoding a C-terminally DsRed2-tagged JP-45, termed JP-45–DsRed2, and an N-terminally EGFP-tagged JP-45, termed GFP–JP-45. The plasmids were generated in Basel and shipped to Ulm for expression and functional testing.

Nuclear injection of plasmids

DNA solutions in sterile water (Aqua ad iniectabilia, Braun, Melsungen, Germany) were diluted to a final concentration of $0.125\,\mu g\,\mu l^{-1}$ for pEGFP-C1 and pDsRed2-N3, to $0.25\,\mu g\,\mu l^{-1}$ for pJP-45–DsRed2 and pEGFP–JP-45 and to $0.5\,\mu g\,\mu l^{-1}$ for pGFP-α_{1C} (Beam & Franzini-Armstrong, 1997). Injection capillaries (Femtotips, Eppendorf, Hamburg, Germany) were filled with the DNA solution and a commercial micro-injection system (Injectman NI 2 micromanipulator and Femtojet pressure delivering device, Eppendorf) was used to inject into myotubes. Injections were performed into one nucleus per myotube by applying a 200-hPa pressure pulse of 0.3-s duration. A successful injection was indicated by a slight swelling and brighter appearance of the nucleus. Cells were placed in Hepes-buffered medium before performing injections; afterwards, the medium was exchanged for normal differentiation medium. Cells were voltage clamped 48 h later.

Confocal imaging

To image cells expressing fluorescent fusion proteins we used a Radiance 2000 confocal scanner (Bio-Rad, Hemel Hempstead, UK) adapted to an Eclipse TE300 inverted fluorescence microscope (Nikon). GFP fluorescence was excited by an Argon laser (488 nm) and filtered by an HQ 515/30 nm emission filter while for the DsRed2 fluorescence, a green He–Ne laser (543 nm) and an E 570 LP emission filter were used. The Argon and He–Ne lasers had nominal powers of 13 and 2.5 mW, respectively, and were used at 10–25% and 60–80% of their maximal power, respectively. Image acquisition was performed using LaserSharp 2000 (Bio-Rad).

Electrophysiology

The experimental solutions had the following compositions. External solution (mM): tetraethyl-ammonium hydroxide (TEAOH) 130, HCl 127, $CaCl_2$ 10, $MgCl_2$ 1, 4-aminopyridine 2.5, glucose 5, tetrodotoxin (TTX) 0.00125 and Hepes 10; pH adjusted to 7.4 with HCl. Internal (pipette) solution (mM): CsOH 145, aspartic acid 135, EGTA 5, HCl 2, Hepes 10, $CaCl_2$ 0.5 (free Ca^{2+}, 10^{-5}), Na_2ATP 0.84, MgATP 4.16 (Mg : ATP ratio (according to supplier), 1.4; free Mg^{2+}, 1), sodium creatine phosphate 5 and K_5-fura-2 0.2; pH adjusted to 7.2 with CsOH. The program CalcV22 (Föhr *et al.* 1993)

was used to calculate the free ion concentrations in the internal solution.

Whole-cell patch-clamp experiments were performed at room temperature (20–23°C) as described by Schuhmeier *et al.* (2003) and Schuhmeier & Melzer (2004). Cells expressing fluorescence from the marker proteins (see below) were further selected for compact shape suitable for single-electrode voltage clamping. Leak resistance and capacitance were determined by applying small positive and negative voltage steps (amplitude, 10 mV; duration, 25 ms) from the holding potential of −90 mV. Correction of residual linear current components (leak and capacitive) not compensated by the analog electronics was performed by using a control pulse from −90 to −110 mV applied 400 ms before each test pulse. Non-linear charge movements were determined by integrating the early transient outward component of the leak and linear capacitance-corrected current traces.

Current recordings $I(V)$ were normalized by the linear capacitance to obtain current densities $i(V)$. The voltage-dependence of the Ca^{2+} current density $i_{Ca}(V)$ was least squares-fitted with eqn (1) and eqn (2):

$$I_{Ca}(V) = f(V)g_{Ca,max}(V - V) \quad (1)$$

$$f(V) = \frac{1}{1 + \exp((V_{0.5} - V)/k)} \quad (2)$$

where $g_{Ca,max}$ and V_{Ca} are maximal normalized conductance and reversal potential, respectively, of the L-type Ca^{2+} current, $f(V)$ is the voltage dependence of activation, $V_{0.5}$ is the voltage of half maximal activation and k determines voltage sensitivity.

Fluorimetry and analysis of Ca^{2+} signals

For the observation of intracellular GFP fluorescence in the patch-clamp experiments, we used an excitation filter BP 470/20, a beam splitter FT 493 and an emission filter BP 505–530 (all Zeiss). For identification of DsRed2 fluorescence in cells, an excitation filter HQ 545/30 (AHF, Tübingen), a beam splitter Q 570 LP (Zeiss) and an emission filter HQ 610/75 (Zeiss) were used. Myotubes were loaded with fura-2 by diffusion from the patch-pipette containing internal solution (see above). Ca^{2+}-dependent fluorescence changes excited at 380 nm (F_{380}) were recorded at 515 nm. After background correction, the F_{380} recordings were normalized by measurements of fluorescence excited at 360 nm (F_{360}), which preceded each voltage-clamp activation as described by Schuhmeier *et al.* (2003). The flux of Ca^{2+} mobilization (Ca^{2+} input flux) during depolarizations was calculated using a Ca^{2+}-binding model (Schuhmeier & Melzer, 2004). The model contained the indicator dye described by fluorescence ratio ($R = F_{380}/F_{360}$) at zero dye saturation (R_{min}), ratio at full dye saturation (R_{max}), rate constants $k_{on,Dye}$, $k_{off,Dye}$ and dye concentration $[Dye]_{total}$, a saturating buffer (S) representing EGTA (parameters $k_{on,S}$, $k_{off,S}$ and $[S]_{total}$) and an uptake mechanism (rate constant k_{uptake}). $[Dye]_{total}$ and $[S]_{total}$ were set to values of 0.2 mM, and 5 mM, respectively. Traces generated with this model were least squares-fitted to the relaxation phases of consecutive voltage-activated fluorescence transients by optimizing the parameters $k_{off,Dye}$, $k_{on,S}$, $k_{off,S}$ and k_{uptake}. For the determination of input flux, the free concentration of myoplasmic Ca^{2+} and the estimated occupancies of the model compartments were summed and the time derivative calculated. Free Ca^{2+} concentration was determined using background- and bleaching-corrected fura-2 fluorescence ratio signals and included reversal of the filtering effect resulting from the binding kinetics of the indicator (Klein *et al.* 1988). For R_{min}, R_{max} and the dissociation constant of the dye ($K_{Dye} = k_{off,Dye}/k_{on,Dye}$) the following values were used: 2.84, 0.68 and 276 nM, respectively. Differential equations were solved using Euler's method. Recordings were smoothed by a digital filter that adjusts its bandwidth automatically to the signal dynamics (for a detailed description of the procedures see Schuhmeier *et al.* 2003 and Schuhmeier & Melzer, 2004).

General analysis and statistics

General calculations and non-linear curve fitting were performed using Excel (Microsoft). Data are presented and plotted as means ± S.E.M. (n = number of experiments) for averaged values, if not indicated otherwise. To compare average values of two independent data sets, Student's t test was used to identify statistically significant differences ($P = 0.05$).

Results

C2C12 myotubes for functional expression studies in EC coupling

In the present study we used C2C12 cells to investigate effects of the junctional face protein JP-45 on voltage-dependent Ca^{2+} signalling in myotubes. C2C12 myotubes express characteristic muscle proteins (Blau *et al.* 1983) and show voltage-activated Ca^{2+} inward current and Ca^{2+} release flux similar to adult skeletal muscle cells (Schuhmeier *et al.* 2003; Schuhmeier & Melzer, 2004).

For heterologous expression of proteins in C2C12 myotubes, we initially examined two frequently applied transfection methods, using calcium phosphate precipitation and Fugene 6 (Roche). Subsequently we tried nuclear injection of the cDNA-carrying plasmids. The effectiveness was tested with mammalian expression

plasmids encoding the fluorescent proteins EGFP and DsRed2 (pEGFP-C1 and pDsRed2-N3, respectively). Of the three methods tested, nuclear injection led to the highest efficiency. The percentage of injected cells expressing the fluorescent marker varied between 10% and 75%. Expression started earlier (∼6 h) compared to cDNA-carrier transfection (∼24 h). We therefore used the nuclear injection for all experiments presented in this study.

Examples of myotubes expressing EGFP and DsRed2, respectively, are shown in Fig. 1*A* and *B*. Both fluorescent proteins exhibited a rather homogeneous distribution in the cytoplasm, as expected for soluble proteins. Figure 1*C* shows the result of injecting the plasmid pDsRed2-ER designed for fluorescent labelling of the endoplasmic reticulum (ER) in living cells. The DsRed2-ER subcellular marker is composed of the targeting signal sequence of calreticulin, the DsRed2 fluorescent protein coding sequence and the KDEL retention signal of calreticulin (Barton & MacLennan, 2004). The KDEL sequence is recognized by receptors, present in vesicular tubular clusters of the ER and the Golgi apparatus, that capture soluble ER resident proteins and carry them back to the ER (Pelham, 1998).

In our C2C12 myotubes, DsRed2-ER labelled a network distributed throughout the cytoplasm, which was denser in the vicinity of the nucleus (Fig. 1*C*). A similar 'net-like' pattern of fluorescence expression was seen when pEGFP–JP-45 (Fig. 1*D*) or pJP-45–DsRed2 (Fig. 1*E*) were injected. This is consistent with JP-45 being expressed in ER membranes as indicated by Anderson *et al.* (2003) for COS-7 cells transfected with pEGFP–JP-45. To obtain further information on the subcellular distribution of JP-45, we coinjected pEGFP–JP-45 and pDsRed2-ER. At 12 h after injection, green and red fluorescence were found to be colocalized in the vicinity of the injected nucleus (not shown). However, later (at 18 and 48 h), the fluorescent patterns were different from each other (Fig. 1*F*). Previous studies suggest that the ER is transformed during differentiation into the functionally distinct SR through gradual replacement of generic ER proteins with specific SR proteins (Villa *et al.* 1993; Sanger *et al.* 2004). Our observations are consistent with JP-45 being generated in the ER and then being targeted to specialized regions of this compartment, whereas DsRed2-ER is retained in the original ER by the KDEL retrieval system.

Test for functional expression

The imaging results described above indicated strong heterologous protein expression in the C2C12 myotubes

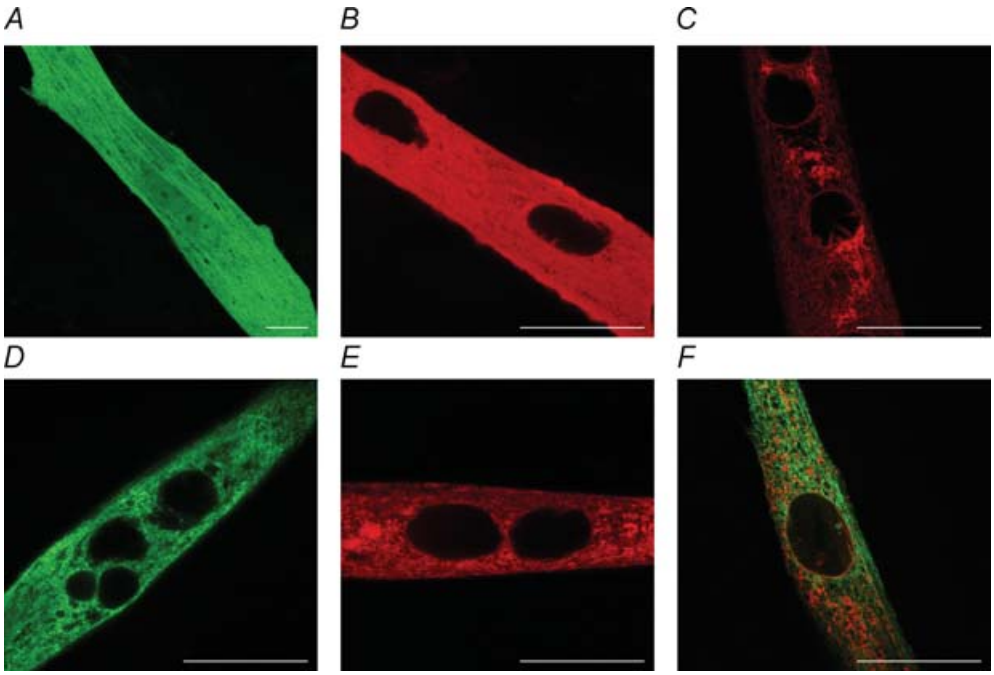

Figure 1. Expression of fluorescent proteins in C2C12 myotubes
Confocal *xy* images showing expression of various fluorescent proteins in C2C12 myotubes. The following plasmids were injected into a single nucleus of each of the displayed myotubes (see Methods for details of injection and imaging conditions): pEGFP-C1 (*A*); pDsRed2-N3 (*B*); pDsRed2-ER (*C*); pEGFP–JP-45 (*D*); pJP-45–DsRed2 (*E*); and pEGFP–JP-45 and pDsRed2-ER (*F*). Pictures were taken 24 h after injection, except for the co-expression experiment in *F* where the waiting time was 18 h. Scale bars indicate 25 μm.

after nuclear plasmid injection. In addition, we performed tests with a construct of well-defined function to verify that the degree of fluorescence expression that we achieved leads to sufficient functional expression. For this purpose, we injected pGFP-α_{1C} that encodes a fluorescent fusion protein of the α_1-subunit of the cardiac L-type Ca^{2+} channel ($Ca_V1.2$). These channels exhibit rapid activation kinetics so that their current can be easily distinguished from the very slowly activating current generated by the intrinsic $Ca_V1.1$ channels (see for example Schuhmeier *et al.* 2005). Figure 2*A* shows a C2C12 myotube that had been injected with the pGFP-α_{1C} plasmid 2 days before imaging. The expression of fluorescent GFP-α_{1C} occurred later in time (2 days) than GFP alone (~6 h) due to its much larger size (217 *versus* 27 kDa) and showed a particulate pattern and a final localization predominantly near the periphery of the cell.

The expression of the green fluorescence from GFP-α_{1C} was accompanied by a significant change in the inward current that could be recorded from the myotubes (Fig. 2*B* and *C*). In the control cells (Fig. 2*B*), the endogenous Ca^{2+} current showed its typical slow activation and no inactivation during the pulse. The currents of the pGFP-α_{1C}-expressing cells (Fig. 2*C*) were larger, became considerably more rapidly activated and showed some degree of inactivation during the pulse.

Figure 2*D* shows the mean voltage dependence of current density at the peak of activation in non-injected control cells (○) and in pGFP-α_{1C}-expressing cells (●). Figure 2*E* shows the voltage dependence of the activation kinetics as determined by a single exponential fit between 5 and 50 ms during the pulse for GFP-α_{1C}-expressing cells (●) and between 20 and 100 ms for control cells (○). On average, at +30 mV (i.e. close to the voltage that produces the maximum inward current) the amplitude was 2.6-fold larger in pGFP-α_{1C}-expressing myotubes and the time constant of activation was 12-fold smaller (data see legend). Thus, Fig. 2 confirms that our procedure allows substantial functional over-expression of even large proteins within the available time frame.

L-type Ca^{2+} current in JP-45 over-expressing cells

Whole-cell patch-clamp experiments were subsequently carried out on myotubes injected with plasmids encoding a fluorescent JP-45 fusion protein. In parallel to the Ca^{2+} currents, intracellular fura-2 Ca^{2+} transients were recorded as described by Schuhmeier & Melzer (2004). We chose DsRed2 as the marker protein (plasmid pJP-45–DsRed2) which exhibits red-shifted fluorescence spectra compared to fura-2. Myotubes injected with pDsRed2-N3, encoding DsRed2 alone, served as controls.

Figure 3*A* and *B* shows examples of Ca^{2+} inward current recordings from two myotubes expressing DsRed2 and JP-45–DsRed2, respectively. Figure 3*C* compares the mean L-type Ca^{2+} current densities measured in the two groups of cells (controls, ○; JP-45–DsRed2, ●). At none of the potentials could a significant difference be observed. Likewise, none of the parameters determined by fitting eqns (1) and (2) to the data in Fig. 3*C* (continuous lines)

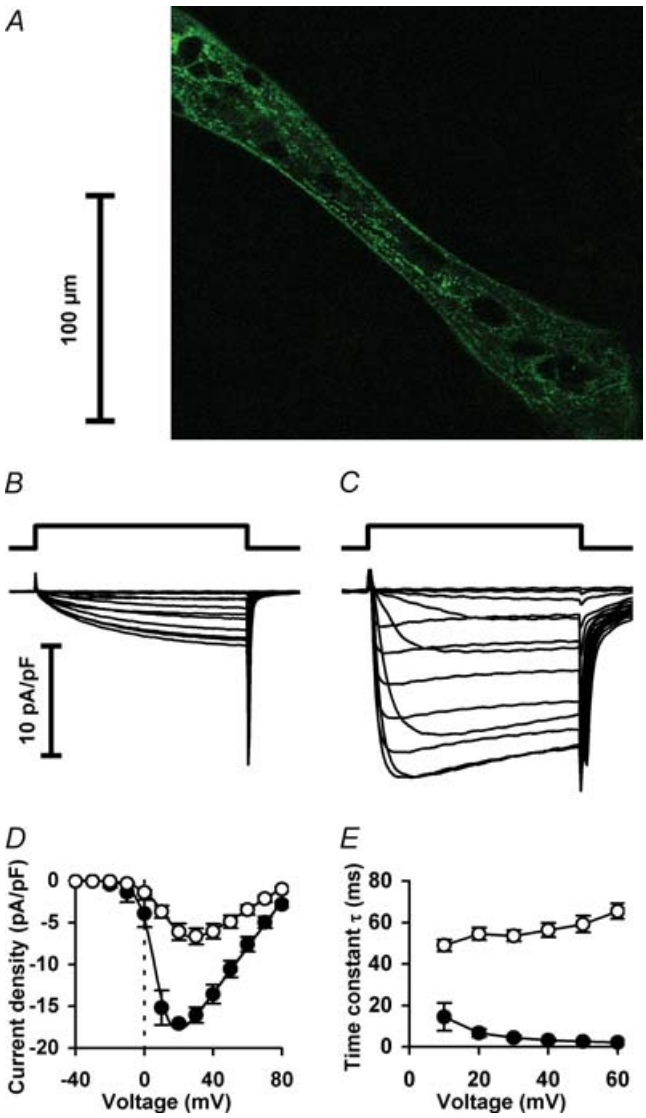

Figure 2. Altered Ca^{2+} inward current in C2C12 myotubes injected with expression plasmids encoding $Ca_v1.2$
A, confocal *xy* image of a myotube expressing GFP-α_{1C}. *B* and *C*, Ca^{2+} inward currents recorded from a non-injected C2C12 myotube and a pGFP-α_{1C}-injected myotube, respectively. Test pulses (200 ms) from a holding potential of −90 mV to voltages between −40 and +80 mV were applied in 10-mV increments. *D*, average of current densities of five control cells (○) and two pGFP-α_{1C}-injected cells (●) at different voltages. *E*, mean time constants of the same sets of cells. The pGFP-α_{1C}-expressing cells display a considerably larger current density (-17.1 ± 0.1 pA pF^{-1}) than the control cells (-6.6 ± 0.9 pA pF^{-1}) and differ from the control cells by the faster kinetics of their inward current. Time constants (τ) were 4.4 ± 1.0 ms and 53.6 ± 2.1 ms at +30 mV, respectively.

Table 1. Best fit results of free parameters in the removal model analysis

Parameters	Units	Schuhmeier & Melzer (2004)	DsRed2-expressing cells	JP45-DsRed2-expressing cells
[EGTA]	mM	15	5	5
$k_{on,Dye}$	$\mu M^{-1}\ s^{-1}$	168.1 ± 6.2	170.6 ± 5.8	180.1 ± 11.7
$k_{off,Dye}$	s^{-1}	46.4 ± 1.7	47.1 ± 2.5	49.7 ± 3.2
$k_{on,S}$	$\mu M^{-1}\ s^{-1}$	20.0 ± 3.6	18.7 ± 3.6	33.0 ± 8.7
$k_{off,S}$	s^{-1}	2.7 ± 0.2	2.9 ± 0.1	3.2 ± 0.3
k_{uptake}	$10^3\ s^{-1}$	10.3 ± 2.3	1.1 ± 0.4	1.9 ± 0.9

Rate constants $k_{off,Dye}$, $k_{on,S}$, $k_{off,S}$ and k_{uptake} of the removal model were optimized by least-squares fitting; $k_{on,Dye}$ was calculated using K_{Dye} and $k_{off,Dye}$. Mean results for DsRed2- ($n = 11$) and JP-45–DsRed2-expressing cells ($n = 6$) are shown in comparison to results of Schuhmeier & Melzer (2004) ($n = 18$). The top row indicates the EGTA concentration in the recording pipette. Data are given as means ± S.E.M.

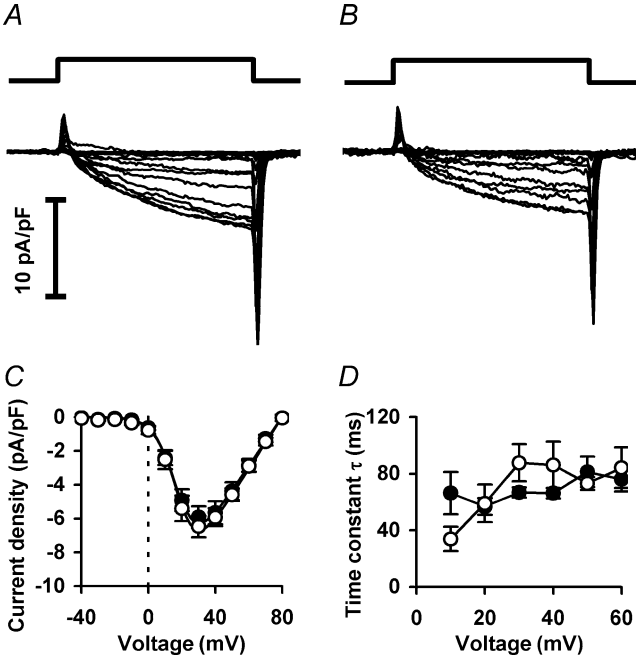

Figure 3. Calcium inward current in JP-45–DsRed2-expressing C2C12 myotubes
Depolarization-activated slow inward currents at different voltages (range −40 to +80 mV) in a myotube expressing DsRed2 (*A*) and in a myotube expressing JP-45–DsRed2 (*B*). *C*, voltage dependence of mean Ca^{2+} current amplitudes, normalized by linear capacitance. The continuous lines are least-squares fits using eqns (1) and (2). Best fit parameters for DsRed2 (○, $n = 11$): $V_{0.5}$, 18.29 ± 1.49 mV; k, 6.22 ± 0.26 mV; $g_{Ca,max}$, 0.16 ± 0.01 S F^{-1}; V_{Ca}, 79.57 ± 1.35 mV; and for JP-45–DsRed2 (●, $n = 6$): $V_{0.5}$, 18.15 ± 1.17 mV; k, 6.62 ± 0.11 mV; $g_{Ca,max}$, 0.15 ± 0.02 S F^{-1}; V_{Ca}, 79.75 ± 1.32 mV. Mean linear capacitance for the same sets of cells was 268.4 ± 5.4 pF (DsRed2) and 296.0 ± 20.7 pF (JP-45–DsRed2). *D*, voltage dependence of mean time constants of activation in the range from +10 to +60 mV. The single-exponential fit of the Ca^{2+} current started 20 ms after the onset of the pulse and ended with the last sampling interval of the pulse.

showed a significant difference. The best fit parameters are listed in the figure legend to Fig. 3.

Figure 3*D* shows the voltage dependence of the activation time constant obtained from single exponential fits to the activation phase of the slow inward current for both DsRed2- and JP-45–DsRed2-expressing cells (○ and ●, respectively). As with current amplitude, no significant difference at any of the investigated voltages could be found.

JP-45 effects on Ca^{2+} release

Each of the cells was analysed using a removal model fit procedure (originally described by Melzer *et al.* 1986). Briefly, this method quantifies Ca^{2+} binding and reuptake parameters of the cell by fitting model-generated traces to the measured fluorescence ratio traces during the time after repolarization (for more details see Schuhmeier & Melzer, 2004). Table 1 lists the mean values of the free kinetic parameters that were adjusted in the removal model to describe the relaxation phases of Ca^{2+} transients for four consecutive voltage pulses of different duration and amplitude. The table shows that the mean values estimated here were similar to data obtained in non-injected myotubes by Schuhmeier & Melzer (2004). Notably, the kinetic data obtained for the indicator dye and for the slow saturable model component S that was included to simulate EGTA were not significantly different. A statistically significant difference from the previous analysis was observed in the rate constant describing slow uptake (k_{uptake}) which might be due to a different pump rate in the present population of cells. Because there were no significant differences in the removal properties of test (JP-45–DsRed2) and control cells (DsRed2), we pooled the removal parameters and used the following set of mean values for further analysis: $k_{on,Dye}$, 175.3 $\mu M^{-1}\ s^{-1}$; $k_{off,Dye}$, 48.4 s^{-1}; $k_{on,S}$, 25.9 $\mu M^{-1}\ s^{-1}$; $k_{off,S}$, 3.1 s^{-1}; k_{uptake}, $1.5 \times 10^3\ s^{-1}$.

Figure 4*Ab* shows a representative fura-2 fluorescence ratio signal obtained during a single application of a 100-ms depolarizing pulse to +30 mV (Fig. 4*Aa*). The signal is drawn inverted in sign so that a rise in Ca^{2+} is upward. The amplitude of the transient was determined by calculating the difference between the average of 20 baseline points and the average of the last six points of the pulse. Figure 4*B* shows the mean amplitudes at different voltages for both DsRed2- (○) and JP-45–DsRed2-expressing (●) myotubes. In the latter set of cells the amplitude was significantly smaller compared to the controls.

Figure 4*Ac* shows the conversion of the fluorescence signal to calcium input flux according to Schuhmeier & Melzer (2004) by using the results of the removal analysis. The arrows in Fig. 4*Ac* indicate the peak of the flux and the plateau, which is reached after the rapid inactivation. Both are plotted as functions of voltage in Fig. 4*C* and *D*. As in Fig. 4*B*, the mean values at +10 mV and above differed significantly in the two groups of cells (except for voltages of +20 and +60 mV).

The sigmoidal voltage dependence in Fig. 4*C* (peaks) was fitted for each individual experiment using a standard Boltzmann equation described by maximum amplitude (A_{max}), $V_{0.5}$ and k. In Fig. 4*D* (plateau) an additional term (as described by Schuhmeier & Melzer, 2004) was added to correct for the gradual decrease in amplitude at large depolarizations. The continuous activation curves in Fig. 4*C* and *D* were calculated using the mean values of the individual fit parameters. Comparing the results for JP-45–DsRed2-expressing myotubes with the controls, there was a significant decrease by 42% for the peak and 44% for the plateau in the parameter describing maximal

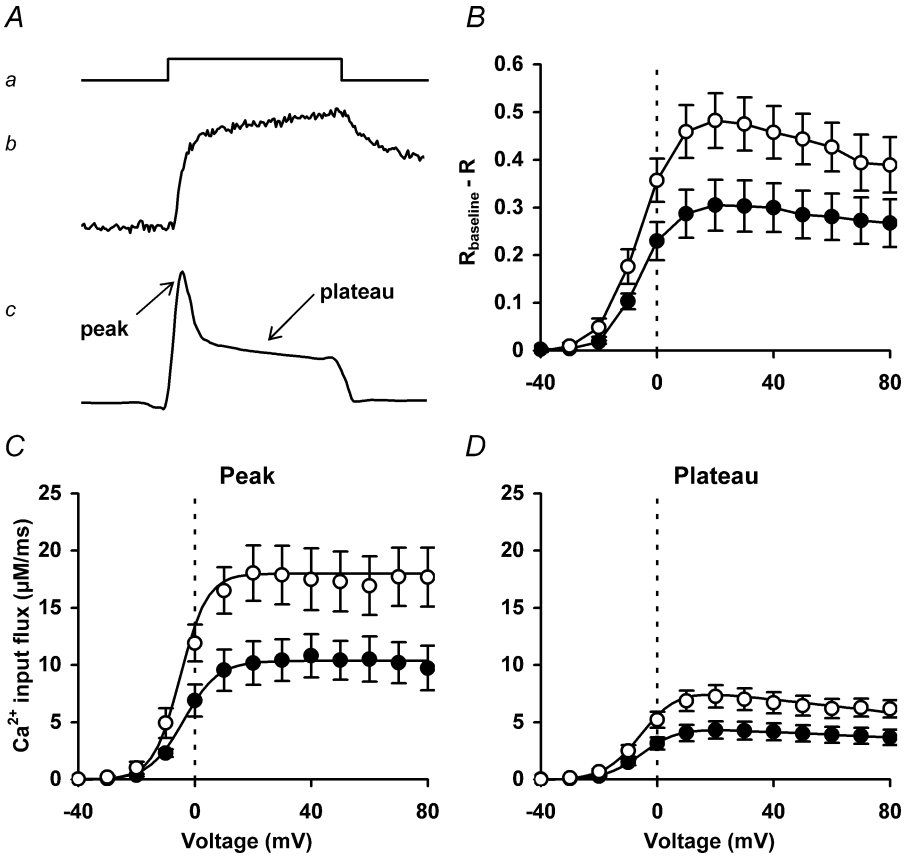

Figure 4. Calcium release in JP-45–DsRed2-expressing C2C12 myotubes
A, example of fluorescence ratio signal (*b*) triggered by a 100-ms depolarization from −90 to +30 mV (*a*); the signal was converted to Ca^{2+} input flux (*c*), using the results of a removal model analysis. *B*, amplitude of the fluorescence ratio signal at the end of the depolarization plotted against voltage for cells expressing DsRed2 (○) and JP-45–DsRed2 (●). *C* and *D*, voltage dependence of peak and plateau Ca^{2+} input flux for the same groups of cells. Plateau is the mean value in an interval of 50 ms centred in the middle of the pulse (indicated by the arrow (plateau) in *c*). Values for $V_{0.5}$, k and A_{max} (see text) of the continuous lines in *C* were −5.03 ± 1.77 mV, 4.58 ± 0.39 mV and 17.99 ± 2.55 μM ms^{-1} for DsRed2 (○) and −3.80 ± 0.87 mV, 5.49 ± 0.63 mV and 10.35 ± 1.86 μM ms^{-1} for JP-45–DsRed2 (●), respectively; the corresponding parameters in *D* were −4.87 ± 1.30 mV, 5.99 ± 0.34 mV and 8.21 ± 1.06 μM ms^{-1} for DsRed2 (○) and −5.06 ± 0.74 mV, 6.16 ± 0.29 mV and 4.59 ± 0.83 μM ms^{-1} for JP-45–DsRed2 (●), respectively. Same sets of cells as in Figure 3.

activation at large depolarizations. All other parameters were not significantly different (see the legend to Fig. 4).

A typical feature of the calculated Ca^{2+} input flux traces was a slowly declining plateau (Fig. 4*Ac* and Fig. 5*A*). In mature muscle, the slope of the plateau has been attributed to progressive SR Ca^{2+} depletion at constant Ca^{2+} release permeability (Schneider *et al.* 1987; Gonzalez & Rios, 1993; Ursu *et al.* 2005). If the initial SR content is known, one can calculate the changes in SR Ca^{2+} content from the estimated Ca^{2+} release flux and correct the flux for SR Ca^{2+} depletion. This leads to an estimate of the voltage-activated SR Ca^{2+} permeability. Under the given assumption, the initial SR Ca^{2+} content can be determined as the value that eliminates the slope in the plateau region when performing the correction. The procedure is demonstrated in Fig. 5 for a series of flux traces obtained at different voltages in a single myotube. At voltages lower than +10 mV, kinetics were slower and the separation between the fast and slow phases of decay (putative inactivation and depletion, respectively) became less obvious in most cells. Therefore, we used the value for SR Ca^{2+} content determined at +10 mV also for depletion correction at voltages below +10 mV. For correction of the flux traces at +10 mV and above, we used the individually determined initial values for SR Ca^{2+} content as described for experiments on adult mouse fibres by Ursu *et al.* (2005).

Figure 6*A* and *B* show the mean results of flux and permeability calculation at +30 mV for all JP-45–DsRed2- and DsRed2- (larger amplitude trace) expressing cells, respectively. The shaded area represents the point-by-point calculated S.E.M. While the fluxes (Fig. 6*A*) showed different time courses due to the faster relative decline during the plateau of the traces with larger amplitudes, permeabilities (Fig. 6*B*) exhibited a very similar time course.

We performed this 'depletion analysis' with the experiments of Fig. 4. Because this procedure is sensitive to any noise disturbing the determination of the slope in the plateau, we had to exclude one recording at +20 mV for DsRed2-expressing cells.

The mean values of the estimated SR Ca^{2+} contents are shown in Fig. 6*C*. The values of mean initial SR Ca^{2+} content at different voltage varied between 1.21 and 1.81 mM and showed no significant difference between JP-45-expressing cells and the controls. Figure 6*D* and *E* shows the voltage dependence of the corrected peak and plateau permeabilities, respectively. Unlike the SR Ca^{2+} content, the permeabilities show significant differences: in Fig. 6*D*, values at −10, 0, +10 and +30 mV are significantly different and in Fig. 6*E*, all values above −20 mV (except for the +20 mV value) are significantly different. Figure 6*F* shows the ratio of peak/plateau, a frequently used measure to characterize the overall shape of the traces. It is essentially constant over the voltage range of activation and not significantly different for JP-45–DsRed2-expressing cells and controls.

To check whether the reduction in voltage-activated Ca^{2+} permeability resulted from a loss of functional voltage sensors, we analysed the non-linear capacitive current at the onset of the depolarization as an estimate of the DHPR gating charge movements. Figure 7*A* and *B* shows the mean values of charge density at different voltages

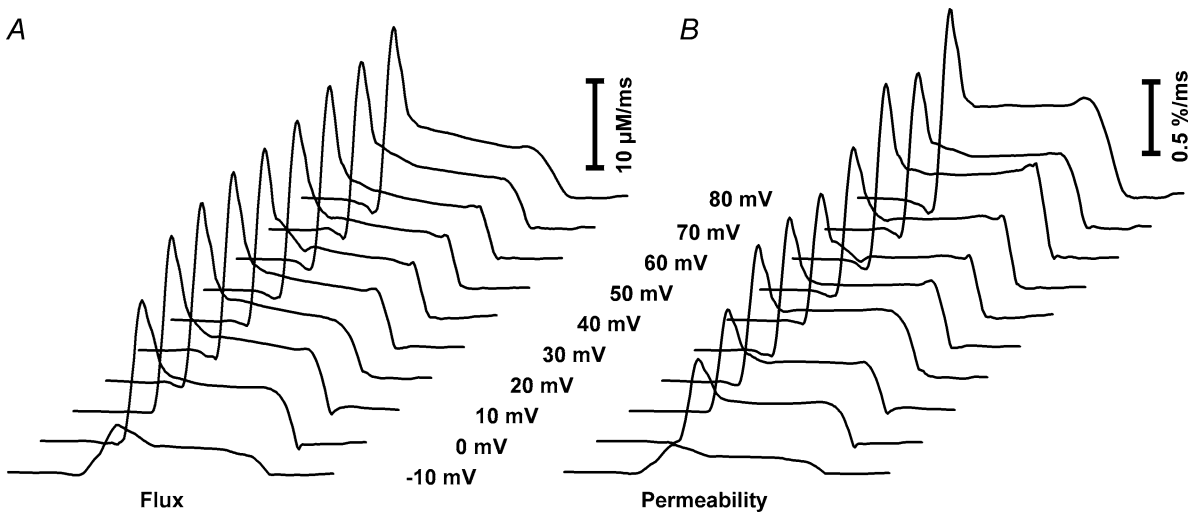

Figure 5. Estimation of Ca^{2+} permeability from Ca^{2+} input flux
Correction of Ca^{2+} input flux traces (*A*) for putative changes in SR Ca^{2+} content at different voltages in a pDsRed2-N3-injected myotube to calculate permeability (*B*). For the depolarizations to +10 mV and more positive voltages, the plateau region of the fluxes in *A* was analysed individually as described in the Results to estimate the initial SR Ca^{2+} content that leads to zero slope during the plateau after correction. The fluxes at the two lowest voltages were corrected using the value of SR Ca^{2+} content estimated at +10 mV.

for myotubes expressing DsRed2 and JP-45–DsRed2, respectively. Consistent with the DHPR-mediated L-type Ca^{2+} current data, no significant difference was found between the two groups of experiments at any voltage. The data were fitted with conventional Boltzmann functions resulting in maximal charge density (q_{max}) values of $10.0 \pm 1.3 \times 10^{-3}$ and $13.0 \pm 2.4 \times 10^{-3}$ C F^{-1} for DsRed2- and JP-45–DsRed2-expressing cells, respectively. The $V_{0.5}$ values were 5.1 ± 1.9 and 6.4 ± 2.1 mV, and the k values 13.1 ± 1.8 and 9.9 ± 1.2 mV ($n = 12$ and $n = 11$), respectively (comp. eqn (2)). A previous study (Zheng *et al.* 2002*a*) obtained mean values of q_{max}, $V_{0.5}$ and k of 6.52 C F^{-1}, 18.7 mV and 14.7 mV, respectively, for control C2C12 myotubes. Note that q_{max} values given in this reference were erroneously scaled up 10-fold (Zheng *et al.* 2002*b* and O. Delbono, personal communication).

Ca^{2+} release flux or Ca^{2+} permeability as a function of the corresponding voltage-sensor charge movement is commonly referred to as the transfer function of EC coupling (e.g. Csernoch *et al.* 1999). Figure 7*C* and *D* show transfer functions using the permeability data of Fig. 6 and the corresponding gating charge densities. Consistent with the lower permeabilities, the transfer functions of the JP-45–DsRed2-expressing cells (Fig. 7*C* and *D*, ●) exhibited considerably lower steepness for both peak (Fig. 7*C*) and plateau permeability (Fig. 7*D*). The average slopes were 84.3 ± 27.0 *versus* $180.9 \pm 40.5\%$ ms^{-1} C^{-1} F ($n = 6$ *versus* $n = 11$, $P = 0.063$) and 39.1 ± 12.5 *versus* $97.0 \pm 21.2\%$ ms^{-1} C^{-1} F ($P = 0.033$), respectively.

These results indicate that the differences in the amplitudes of Ca^{2+} transients and Ca^{2+} flux observed here (Fig. 4) resulted from differences in the activated permeation pathway and not from differences in either the Ca^{2+} gradient that drives the flux or in voltage-sensor properties.

Discussion

In the present study, we searched for possible functional effects of the recently discovered JFM protein JP-45 in myotubes. We focused on the two voltage-controlled fluxes of Ca^{2+}; that is, Ca^{2+} inward current and Ca^{2+} release. Myotubes derived from the C2C12 cell line were used for over-expression of a fusion protein consisting of the fluorescent marker DsRed2 and JP-45. A change in Ca^{2+} release but not in Ca^{2+} current was observed.

Analysis of Ca^{2+} removal and Ca^{2+} release in C2C12 myotubes

To study Ca^{2+} release, we used an adapted version of the removal model fit approach first described by Melzer *et al.* (1986). The values of the binding rate constants identified with this analysis were remarkably similar to those of our

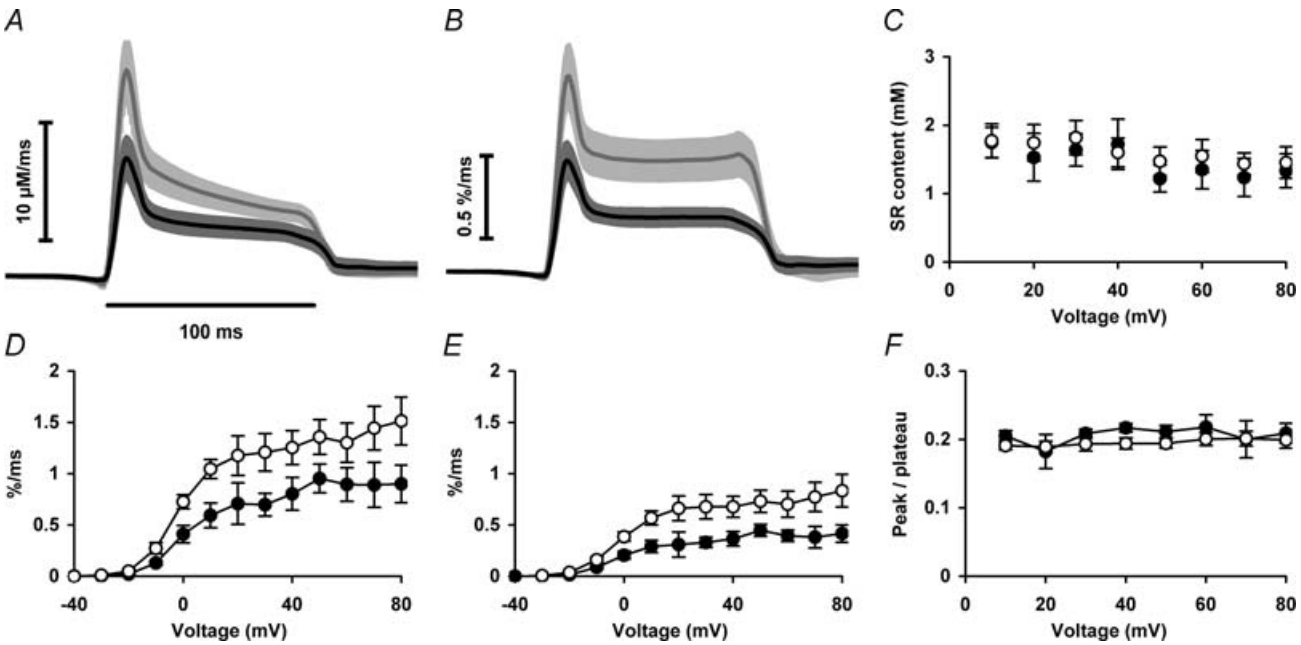

Figure 6. Altered Ca^{2+} permeability in JP-45–DsRed2-expressing C2C12 myotubes
Comparison of mean Ca^{2+} input flux (*A*) and Ca^{2+} permeability (*B*) at +30 mV for DsRed2- (top trace) and JP-45–DsRed2-expressing (bottom trace) myotubes. The point-by-point calculated S.E.M. is indicated by the shaded areas. *C*, estimated initial SR Ca^{2+} content in the voltage range between +10 and +80 mV. *D* and *E*, voltage dependence of peak and plateau permeability, respectively. *F*, ratio of peak/plateau (both measured from the baseline). DsRed2-expressing myotubes, ○; JP-45–DsRed2-expressing myotubes, ●. Same sets of cells as in Figure 3.

previous investigation in C2C12 myotubes (Schuhmeier & Melzer, 2004) despite the lower concentration of EGTA used. DsRed2- and JP-45–DsRed2-expressing cells did not differ significantly in any of the estimated rate constants, indicating that removal properties were not affected by JP-45 and suggesting that the observed difference in Ca^{2+} signal amplitude results from a difference in the Ca^{2+} release activity rather than removal properties.

Ca^{2+} release flux is the product of SR permeability and SR Ca^{2+} content. The method that we used to calculate voltage-activated Ca^{2+} permeability (Schneider *et al.* 1987; Gonzalez & Rios, 1993) estimates the SR Ca^{2+} content prior to the pulse ($Ca_{0,SR}$) and corrects the release flux for the putative changes in SR Ca^{2+} content determined from the flux and its slope during the slow phase. The values of $Ca_{0,SR}$ estimated in our experiments for DsRed2- and JP-45–DsRed2-expressing myotubes averaged over the voltage range +10 to +80 mV (1.60 ± 0.23 and 1.47 ± 0.27 mM, respectively) were not significantly different from each other indicating that loading of the SR was not changed.

In voltage-clamped rat and mouse muscle fibres, values of 1.9 and about 3 mM, respectively, have been determined for $Ca_{0,SR}$ using the same method (Shirokova *et al.* 1996; Ursu *et al.* 2005). It should be noted that $Ca_{0,SR}$ is expressed in concentration with respect to the myoplasmic water volume, as is the release flux. An estimate of the SR volume in relation to myoplasmic water volume would be required (but is not available for myotubes) to convert the numbers to true concentrations in the SR. On the other hand, permeabilities (in % ms^{-1}) and fractional changes of SR Ca^{2+} content are independent of such morphometric data and therefore permit a comparison with data obtained from adult muscle fibres. For the peak permeability values in control myotubes, we obtained about 1.4% ms^{-1} at +50 mV in the present study compared to about 6% ms^{-1} at the same potential in mouse interosseus fibres (Ursu *et al.* 2005). We determined that a 100-ms voltage pulse that maximally activates Ca^{2+} release leads on average to about 50% reduction in the SR Ca^{2+} content of the control (i.e. DsRed2-expressing) C2C12 myotubes. This compares to about 80% in mature mouse fibres estimated by a very similar analysis procedure (Ursu *et al.* 2005).

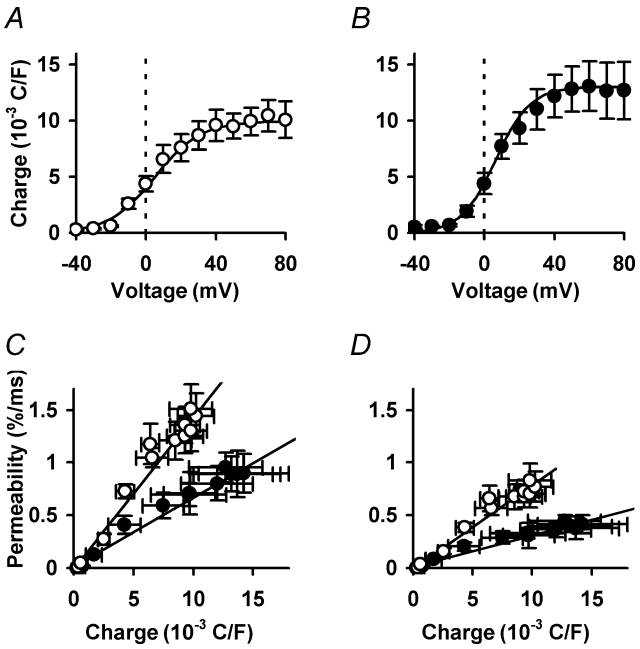

Figure 7. Intramembrane charge movements and EC coupling transfer functions
A and *B*, voltage dependence of charge density in cells expressing DsRed2 (*A*, $n = 12$) and JP-45–DsRed2 (*B*, $n = 11$). Continuous curves are Boltzmann functions fitted to the data. *C* and *D*, transfer functions; that is, peak Ca^{2+} permeability (*C*) and plateau permeability (*D*) plotted against the corresponding charge density. DsRed2-expressing myotubes ($n = 11$), ○; JP-45–DsRed2-expressing myotubes ($n = 6$), ●. Continuous curves are straight lines through the origin fitted to the mean values.

Interpretation of JP-45 effects on Ca^{2+} signalling in C2C12 cells

The localization of the JFM suggests a contribution of JP-45 to the 'Ca^{2+} signalling toolkit' (Berridge *et al.* 2003) of skeletal muscle. Possible roles include participation in the formation of the triadic junction, in targeting one of its constituents to the junction or in modifying EC coupling directly. Results of Anderson (2003) indicated colocalization of JP-45 with ryanodine receptors but no direct interaction with the release channel. Instead, *in vitro* interaction with the α_{1S} subunit of the DHPR has been reported (AA Anderson, X Altafaj, Z Zheng, Z-M Wang, O Delbono, M Ronjat, S Treves, F Zorzato, 2003), making JP-45 an interesting candidate for a possible functional modulator of EC coupling. Recent experimental evidence also suggests an interaction with the β subunit of the DHPR (Anderson *et al.* unpublished results). Modulation of the DHPR might affect its voltage-sensing properties, the size of the Ca^{2+} entry flux or the conformational transmission to the RyR. Experiments correlating maximum charge movement with the JP-45–DsRed2 fluorescence level in transfected cells indicated a decrease at high expression levels (AA Anderson, X Altafaj, Z Zheng, Z-M Wang, O Delbono, M Ronjat, S Treves, F Zorzato unpublished results). Our set-up was not equipped for quantifying Ca^{2+} signals and JP-45–DsRed2 fluorescence simultaneously. Because under the present conditions we found no evidence for altered charge movements, we suspect that the expression levels reached in our case are below the values needed to affect charge movements significantly. Nevertheless, our study showed a reduction in the Ca^{2+} signals and in the calculated flux of Ca^{2+} mobilization. The lower effectiveness of voltage-sensor charge movements in activating SR permeability, indicated by the reduced slope of the EC coupling transfer functions

(Fig. 7*C* and *D*), may have resulted from an inhibiting effect on the transmission from the DHPR caused by the interaction of the N-terminal region of JP-45 with the DHPR (Anderson *et al.* 2003). Alternatively, it may have resulted from an interaction of the luminal C-terminal end of JP-45 with CSQ, as demonstrated *in vitro* (Anderson *et al.* 2003). This interaction might affect the Ca^{2+} storing properties in the lumen of the SR by altering the buffer capacity of CSQ. Yet, our analysis of $Ca_{0,SR}$ (see above) showed no evidence for a reduced Ca^{2+} concentration in the SR. In heart muscle, three proteins of the JFM (i.e. RyR, triadin and junctin) form a complex with CSQ that seems to influence the open probability of the RyR as a function of the Ca^{2+} concentration in the SR lumen (Zhang *et al.* 1997; Györke *et al.* 2004). In this complex, CSQ has been proposed to serve as a Ca^{2+} sensor that modulates the RyR via links formed by triadin and junctin. A similar complex appears to be present in skeletal muscle (Beard *et al.* 2005) and may serve equivalent regulatory functions that may be altered by JP-45. Even though this indirect mechanism cannot be ruled out, in our opinion it is less likely than a more direct effect of JP-45 on functional domains of the DHPR relevant for Ca^{2+} release control.

JP-45 is specific for skeletal muscle SR. Therefore based on our results, it seems likely that JP-45 down-regulates the multiprotein EC coupling complex of the terminal cisternae in a manner specific to skeletal muscle. Consequently, loss of function by mutations in JP-45 may lead to skeletal muscle-specific pathological over-activity of the Ca^{2+} release system. Mutations in RyR1 that lead to increased Ca^{2+} release are known to cause malignant hyperthermia susceptibility (MHS) or central core disease (CCD). Therefore it seems worthwhile to screen the sequence of human JP-45 for mutations in those families with MHS or CCD with no known RyR1 mutations (Jurkat-Rott *et al.* 2000; Lyfenko *et al.* 2004). Further important clues about the role of the protein can be expected from experiments similar to the ones shown here performed on myotubes or adult muscle fibres of genetically altered mice lacking JP-45.

In summary, we demonstrated, using plasmids encoding fluorescent fusion proteins, that efficient and rapid protein expression can be achieved in C2C12 myotubes by nuclear microinjection. Fusion constructs of JP-45, a protein of the skeletal muscle SR junctional face, expressed strong fluorescence in a cellular membrane compartment distinct from the ER portion labelled by DsRed2-ER. Using fura-2 fluorimetry under whole-cell voltage-clamp conditions, we found that JP-45–DsRed2-expressing C2C12 myotubes exhibited a decrease in depolarization-induced Ca^{2+} transients while Ca^{2+} inward current density was unaltered. Using a procedure to determine Ca^{2+} flux and permeability from the Ca^{2+} transient, the change could be tentatively assigned to an effect on the Ca^{2+} permeability of the SR rather than its Ca^{2+} content. Because *in vitro* studies had demonstrated binding of JP-45 to both the DHPR and calsequestrin, the observed effect on Ca^{2+} release may be attributed to a modulatory effect of either one of these interactions.

References

Anderson AA, Treves S, Biral D, Betto R, Sandona D, Ronjat M & Zorzato F (2003). The novel skeletal muscle sarcoplasmic reticulum JP-45 protein. Molecular cloning, tissue distribution, developmental expression, and interaction with alpha 1.1 subunit of the voltage-gated calcium channel. *J Biol Chem* **278**, 39987–39992.

Arikkath J & Campbell KP (2003). Auxiliary subunits: essential components of the voltage-gated calcium channel complex. *Curr Opin Neurobiol* **13**, 298–307.

Barton K & MacLennan D (2004). The proteins of sarcotubular system. In *Myology: Basic and Clinical*, 3rd edn, ed. Engel AG & Franzini-Armstrong C, pp. 307–323. McGrow Hill, New York.

Beam KG & Franzini-Armstrong C (1997). Functional and strutural approaches to the study of EC coupling. In *Methods in Muscle Biology*, ed. Emerson C & Sweeney H, pp. 284–306. Academic Press, San Diego.

Beard NA, Casarotto MG, Wei L, Varsanyi M, Laver DR & Dulhunty AF (2005). Regulation of ryanodine receptors by calsequestrin: effect of high luminal Ca^{2+} and phosphorylation. *Biophys J* **88**, 3444–3454.

Berridge MJ, Bootman MD & Roderick HL (2003). Calcium signalling: dynamics, homeostasis and remodelling. *Nat Rev Mol Cell Biol* **4**, 517–529.

Bers DM (2001). *Excitation-Contraction Coupling and Cardiac Contractile Force*, 2nd edn, ed. Kluwer Academic Publishers, Dordrecht.

Blau HM, Webster C & Pavlath GK (1983). Defective myoblasts identified in Duchenne muscular dystrophy. *Proc Natl Acad Sci U S A* **80**, 4856–4860.

Brum G, Stefani E & Rios E (1987). Simultaneous measurements of Ca^{2+} currents and intracellular Ca^{2+} concentrations in single skeletal muscle fibers of the frog. *Can J Physiol Pharmacol* **65**, 681–685.

Caswell AH, Brandt NR, Brunschwig JP & Purkerson S (1991). Localization and partial characterization of the oligomeric disulfide-linked molecular weight 95,000 protein (triadin) which binds the ryanodine and dihydropyridine receptors in skeletal muscle triadic vesicles. *Biochemistry* **30**, 7507–7513.

Csernoch L, Szentesi P & Kovacs L (1999). Differential effects of caffeine and perchlorate on excitation-contraction coupling in mammalian skeletal muscle. *J Physiol* **520**, 217–230.

Föhr KJ, Warchol W & Gratzl M (1993). Calculation and control of free divalent cations in solutions used for membrane fusion studies. *Methods Enzymol* **221**, 149–157.

Friedrich O, Ehmer T & Fink RH (1999). Calcium currents during contraction and shortening in enzymatically isolated murine skeletal muscle fibres. *J Physiol* **517**, 757–770.

Gonzalez A & Rios E (1993). Perchlorate enhances transmission in skeletal muscle excitation-contraction coupling. *J Gen Physiol* **102**, 373–421.

Grabner M, Dirksen RT & Beam KG (1998). Tagging with green fluorescent protein reveals a distinct subcellular distribution of L-type and non-L-type Ca^{2+} channels expressed in dysgenic myotubes. *Proc Natl Acad Sci U S A* **95**, 1903–1908.

Guo W & Campbell KP (1995). Association of triadin with the ryanodine receptor and calsequestrin in the lumen of the sarcoplasmic reticulum. *J Biol Chem* **270**, 9027–9030.

Györke I, Hester N, Jones LR & Györke S (2004). The role of calsequestrin, triadin, and junctin in conferring cardiac ryanodine receptor responsiveness to luminal calcium. *Biophys J* **86**, 2121–2128.

Jones LR, Zhang L, Sanborn K, Jorgensen AO & Kelley J (1995). Purification, primary structure, and immunological characterization of the 26-kDa calsequestrin binding protein (junctin) from cardiac junctional sarcoplasmic reticulum. *J Biol Chem* **270**, 30787–30796.

Jurkat-Rott K, McCarthy T & Lehmann-Horn F (2000). Genetics and pathogenesis of malignant hyperthermia. *Muscle Nerve* **23**, 4–17.

Klein MG, Simon BJ, Szücs G & Schneider MF (1988). Simultaneous recording of calcium transients in skeletal muscle using high- and low-affinity calcium indicators. *Biophys J* **53**, 971–988.

Knudson CM, Stang KK, Jorgensen AO & Campbell KP (1993). Biochemical characterization of ultrastructural localization of a major junctional sarcoplasmic reticulum glycoprotein (triadin). *J Biol Chem* **268**, 12637–12645.

Lyfenko AD, Goonasekera SA & Dirksen RT (2004). Dynamic alterations in myoplasmic Ca^{2+} in malignant hyperthermia and central core disease. *Biochem Biophys Res Commun* **322**, 1256–1266.

MacKrill JJ (1999). Protein–protein interactions in intracellular Ca^{2+}-release channel function. *Biochem J* **337**, 345–361.

Melzer W, Herrmann-Frank A & Lüttgau HC (1995). The role of Ca^{2+} ions in excitation-contraction coupling of skeletal muscle fibres. *Biochim Biophys Acta* **1241**, 59–116.

Melzer W, Rios E & Schneider MF (1986). The removal of myoplasmic free calcium following calcium release in frog skeletal muscle. *J Physiol* **372**, 261–292.

Pelham HR (1998). Getting through the Golgi complex. *Trends Cell Biol* **8**, 45–49.

Sanger JW, Sanger JM & Franzini-Armstrong C (2004). Assembly of the skeletal muscle. In *Myology: Basic and Clinical*, 3rd edn, ed. Engel AG & Franzini-Armstrong C, pp. 45–65. McGrow Hill, New York.

Schneider MF, Simon BJ & Szücs G (1987). Depletion of calcium from the sarcoplasmic reticulum during calcium release in frog skeletal muscle. *J Physiol* **392**, 167–192.

Schuhmeier RP, Dietze B, Ursu D, Lehmann-Horn F & Melzer W (2003). Voltage-activated calcium signals in myotubes loaded with high concentrations of EGTA. *Biophys J* **84**, 1065–1078.

Schuhmeier RP, Gouadon E, Ursu D, Kasielke N, Flucher BE, Grabner M & Melzer W (2005). Functional interaction of CaV channel isoforms with ryanodine receptors studied in dysgenic myotubes. *Biophys J* **88**, 1765–1777.

Schuhmeier RP & Melzer W (2004). Voltage-dependent Ca^{2+} fluxes in skeletal myotubes determined using a removal model analysis. *J Gen Physiol* **123**, 33–51.

Shirokova N, Garcia J, Pizarro G & Rios E (1996). Ca^{2+} release from the sarcoplasmic reticulum compared in amphibian and mammalian skeletal muscle. *J Gen Physiol* **107**, 1–18.

Szentesi P, Collet C, Sarkozi S, Szegedi C, Jona I, Jacquemond V, Kovacs L & Csernoch L (2001). Effects of dantrolene on steps of excitation-contraction coupling in mammalian skeletal muscle fibers. *J Gen Physiol* **118**, 355–375.

Ursu D, Schuhmeier RP & Melzer W (2005). Voltage-controlled Ca^{2+} release and entry flux in isolated adult muscle fibres of the mouse. *J Physiol* **562**, 347–365.

Villa A, Podini P, Nori A, Panzeri MC, Martini A, Meldolesi J & Volpe P (1993). The endoplasmic reticulum-sarcoplasmic reticulum connection. II. Postnatal differentiation of the sarcoplasmic reticulum in skeletal muscle fibers. *Exp Cell Res* **209**, 140–148.

Walker D & De Waard M (1998). Subunit interaction sites in voltage-dependent Ca^{2+} channels: role in channel function. *Trends Neurosci* **21**, 148–154.

Zhang L, Kelley J, Schmeisser G, Kobayashi YM & Jones LR (1997). Complex formation between junctin, triadin, calsequestrin, and the ryanodine receptor. Proteins of the cardiac junctional sarcoplasmic reticulum membrane. *J Biol Chem* **272**, 23389–23397.

Zheng Z, Wang ZM & Delbono O (2002*a*). Charge movement and transcription regulation of L-type calcium channel alpha (1S) in skeletal muscle cells. *J Physiol* **540**, 397–409.

Zheng Z, Wang ZM, Delbono O (2002*b*). Erratum for Zheng *et al*. *J Physiol* **540**, 397–409. *J Physiol* **541**, 1059.

Zorzato F, Anderson AA, Ohlendieck K, Froemming G, Guerrini R & Treves S (2000). Identification of a novel 45 kDa protein (JP-45) from rabbit sarcoplasmic-reticulum junctional-face membrane. *Biochem J* **351**, 537–543.

Acknowledgements

We thank E. Schoch for designing and constructing equipment and A. Riecker and K. Nothelfer for expert technical help. We are grateful to M. Grabner and B. E. Flucher (Innsbruck) and to H. Lerche and S. Maljevic (Ulm) for providing mammalian expression plasmids. We acknowledge a contribution of the European Commission to W.M. for graduate training (HPRN-CT-2002-00331). E.G. received partial funding from Graduiertenkolleg 460 and Landesschwerpunkt Nanoskopie. The work was funded by a grant of the Deutsche Forschungsgemeinschaft (DFG) to W.M. (ME-713/10-3).